Article



Effects of cholesterol on the structure and collapse of DPPC monolayers

Fazle R. Dayeen, ¹ Bret A. Brandner, ² Michael W. Martynowycz, ³ Kamil Kucuk, ¹ Michael J. Foody, ⁵ Wei Bu, ⁴ Stephen B. Hall, ^{2,*} and David Gidalevitz ^{1,*}

¹Department of Physics, Center for Molecular Study of Condensed Soft Matter (μCoSM), Pritzker Institute of Biomedical Science and Engineering, Illinois Institute of Technology, Chicago, Illinois; ²Pulmonary & Critical Care Medicine, Oregon Health & Science University, Portland, Oregon; ³Howard Hughes Medical Institute and Department of Biological Chemistry, University of California Los Angeles, Los Angeles, California; ⁴NSF's ChemMatCARS, Pritzker School of Molecular Engineering, University of Chicago, Chicago, Illinois; and ⁵Department of Chemistry, Illinois Institute of Technology, Chicago, Illinois

ABSTRACT Cholesterol induces faster collapse by compressed films of pulmonary surfactant. Because collapse prevents films from reaching the high surface pressures achieved in the alveolus, most therapeutic surfactants remove or omit cholesterol. The studies here determined the structural changes by which cholesterol causes faster collapse by films of dipalmitoyl phosphatidyl-choline, used as a simple model for the functional alveolar film. Measurements of isobaric collapse, with surface pressure held constant at 52 mN/m, showed that cholesterol had little effect until the mol fraction of cholesterol, X_{chol} , exceeded 0.20. Structural measurements of grazing incidence X-ray diffraction at ambient laboratory temperatures and a surface pressure of 44 mN/m, just below the onset of collapse, showed that the major structural change in an ordered phase occurred at lower X_{chol} . A centered rectangular unit cell with tilted chains converted to an untilted hexagonal structure over the range of $X_{\text{chol}} = 0.0$ –0.1. For $X_{\text{chol}} = 0.1$ –0.4, the ordered structure was nearly invariant; the hexagonal unit cell persisted, and the spacing of the chains was essentially unchanged. That invariance strongly suggests that above $X_{\text{chol}} = 0.1$, cholesterol partitions into a disordered phase, which coexists with the ordered domains. The phase rule requires that for a binary film with coexisting phases, the stoichiometries of the ordered and disordered regions must remain constant. Added cholesterol must increase the area of the disordered phase at the expense of the ordered regions. X-ray scattering from dipalmitoyl phosphatidylcholine/cholesterol fit with that prediction. The data also show a progressive decrease in the size of crystalline domains. Our results suggest that cholesterol promotes adsorption not by altering the unit cell of the ordered phase but by decreasing both its total area and the size of individual crystallites.

SIGNIFICANCE In vitro studies show that cholesterol in sufficient amounts disrupts the function of pulmonary surfactant. Cholesterol promotes faster desorption from the air/water interface and prevents the films from reaching the high surface pressures achieved in the alveolar air sacks. On that basis, cholesterol is removed or omitted from almost all therapeutic surfactants. Endogenous pulmonary surfactant, however, contains \sim 5%–12% (w:w) cholesterol, suggesting that this compound might not be detrimental. The studies here determined the response of collapse by dipalmitoyl phosphatidylcholine, used as a simple model of the alveolar film, to increasing amounts of cholesterol. We then established what structural alterations could explain those changes. Our results show that cholesterol up to physiological levels has minimal effect on collapse. At the higher levels where collapse does sharply increase, the effect reflects a decrease in the size of individual crystallites and the total area of the condensed phase rather than a change in its molecular structure.

INTRODUCTION

The role of cholesterol in the function of pulmonary surfactant is controversial. Along with phospholipids and small

Submitted April 17, 2022, and accepted for publication July 5, 2022.

*Correspondence: sbh@ohsu.edu or gidalevitz@iit.edu

Fazle R. Dayeen and Bret A. Brandner contributed equally.

Editor: Tommy Nylander.

https://doi.org/10.1016/j.bpj.2022.07.007

© 2022 Biophysical Society.

amounts of specific proteins, pulmonary surfactant contains \sim 5%–12% (w:w) cholesterol (1,2). Biophysical studies have suggested that cholesterol should be functionally detrimental. Pulmonary surfactant forms a thin film on the surface of the liquid layer that lines the alveolar air spaces. When compressed by the shrinking alveolar surface area during exhalation, the film achieves high surface pressures (π) that reduce surface tension to exceptionally low levels, <5 mN/m (3–9). The values of π are well above the



equilibrium spreading pressures (π_e) of \sim 46 mN/m (Fig. 1), at which fluid monolayers coexist with their three-dimensional bulk phase (10). Vesicles in the subphase adsorb only to π_e . If compressed to π just above π_e , fluid films collapse from the interface to form multilamellar stacks (11). When compression stops, π relaxes to π_e (Fig. 1). Cholesterol increases the rates of collapse (12–14). On that basis, cholesterol is removed from almost all therapeutic surfactants obtained from animal sources (15–23) and omitted from artificial preparations (24–27).

A recent study has raised the possibility that, at least in therapeutic surfactants, cholesterol might actually be beneficial. During normal breathing, premature neonates, born before they have adequate amounts of surfactant, develop the injured lungs of the respiratory distress syndrome (28). Administration of exogenous surfactants has improved their survival (29). Instilling the dispersed surfactant as a bulk liquid, however, requires endotracheal intubation. That procedure, particularly for small premature infants in respiratory distress, is hazardous. Several studies have attempted to avoid intubation by instead administering the surfactant as an aerosol (30). An extract of calf surfactant given by

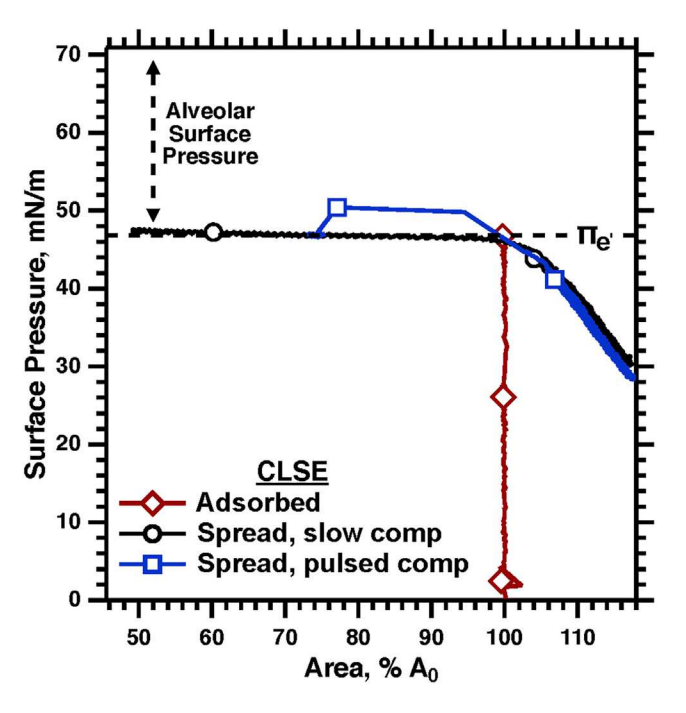


FIGURE 1 Equilibrium spreading pressure (π_e) for films of extracted calf surfactant (calf lung surfactant extract) formed on the surface of captive bubbles. Films achieved the same final π during the following processes: adsorption to a constant surface area; slow compression of a monolayer, spread from organic solvent, across a plateau of relatively constant π , corresponding to collapse; and relaxation of a spread monolayer following a pulsed compression to a π slightly above π_e . Collapse at π_e limits access to the range of alveolar π , indicated by the vertical dashed line. Experimental conditions: temperature, 37°C; subphase, HSC; phospholipid concentration for adsorbed films, 0.5 mM phospholipid; A_0 is the area of the film when $\pi=46$ mN/m; rates of compression: slow, 2.43 min $^{-1}$; pulsed, 14.4 min $^{-1}$. To see this figure in color, go online.

aerosol has now succeeded in improving the survival of babies with or at risk for the respiratory distress syndrome (31). The extracted surfactant contains physiological levels of cholesterol, which should reduce the viscosity of the resulting film. The investigators speculated, without evidence or elaboration, that the viscosity of their preparation might be responsible for its success. Lower viscosity would presumably promote distribution of the inhaled surfactant throughout the lungs.

The role of cholesterol, in both the function of the alveolar film and in therapeutic surfactants, is therefore uncertain. The dose-response to cholesterol may be crucial in answering this question. Below a threshold level, cholesterol has little effect on the stability of films containing extracted surfactant (32). Those results raise the possibility that specific amounts of cholesterol induce a structural alteration, such as a phase transition, that destabilizes compressed films. Below that level, cholesterol might beneficially reduce the viscosity of the film without disrupting its ability to sustain high π . The studies here established how increasing amounts of cholesterol affect the function and structure of dipalmitoyl phosphatidylcholine (DPPC) monolayers. The classical model of pulmonary surfactant has long maintained that to achieve high π , the alveolar film must consist of a condensed phase (33,34), in which acyl chains form a crystalline array (35). That structure resists collapse and sustains high π . DPPC is the only component of pulmonary surfactant that, by itself at physiological temperatures, can form a condensed film (36,37). A corollary of the classical model contends that the content of DPPC in the alveolar film must be high, approaching a pure composition. Measurements here on captive bubbles determined the kinetics of collapse for DPPC with different amounts of cholesterol. Grazing incidence x-ray diffraction (GIXD) at π just below π_e then measured the structural effects of cholesterol. Our results address the extent to which the alteration of ordered structures by that compound can explain the variation of collapse.

MATERIALS AND METHODS

Materials

DPPC was obtained from Avanti Polar Lipids (Alabaster, AL, USA). Cholesterol (purity > 99%) was purchased from Sigma-Aldrich (St. Louis, MO, USA). The composition of the lipid mixtures was expressed as the mol fraction of the steroid ($X_{\rm chol}$). The following items were purchased commercially: high-performance liquid chromatography-grade chloroform and methanol (EMD Millipore, Burlington, MA, USA, and Fisher Scientific, Waltham, MA, USA, respectively); N-2-hydroxyethylpiperazine-N'-2-ethane sulfonic acid (Hepes) (Sigma, St. Louis, MO, USA); and CaCl₂•2H₂O, NaCl (Mallinckrodt, Hazelwood, MO, USA). All of these materials were used without further analysis or purification. Water processed by a Barnstead Nanopure Diamond purification system (Dubuque, IA, USA) had a resistance $\geq 18.2 \text{ M}\Omega$. Buffered electrolyte (HSC) contained 10 mM Hepes (pH 7.0), 150 mM NaCl, and 1.5 mM CaCl₂.

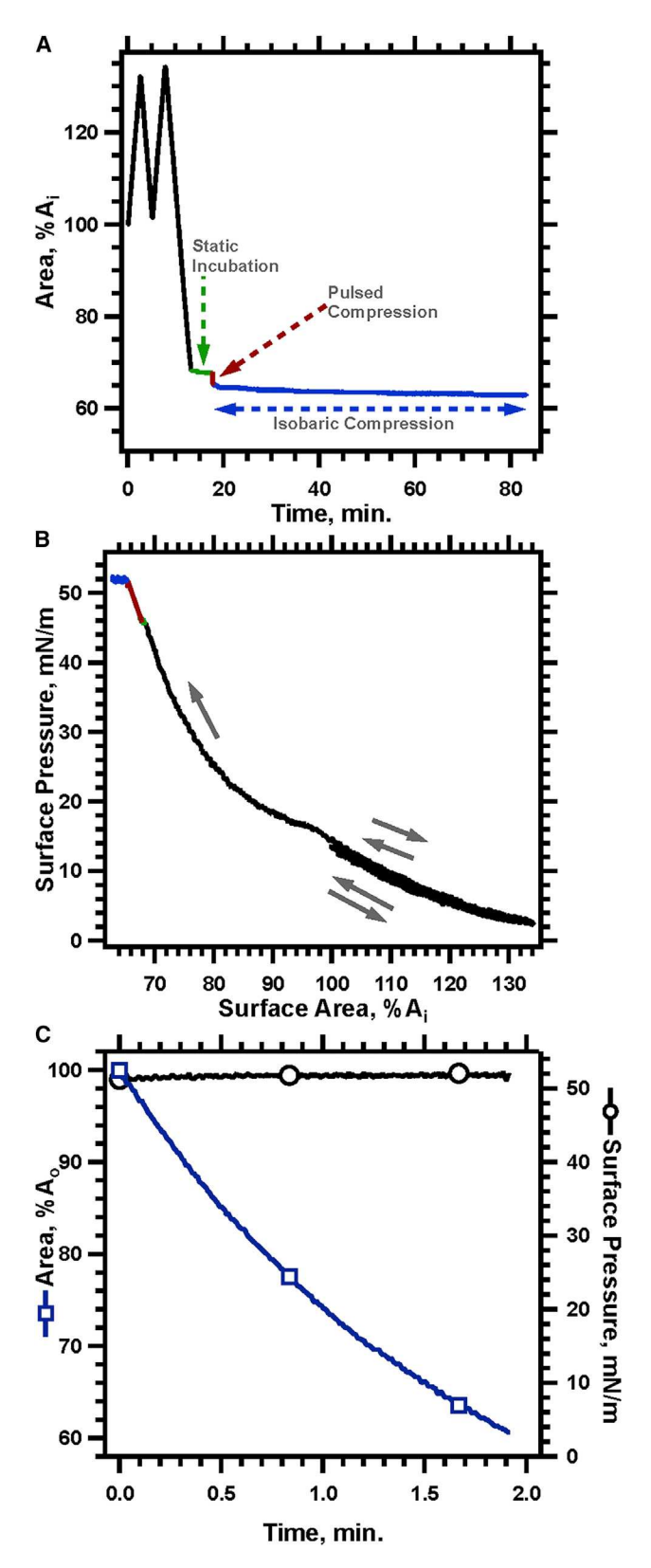


FIGURE 2 Measurements of isobaric compression for cholesterol-DPPC at $X_{\text{chol}} = 0.10$ and 23°C. (A) Temporal variation of surface area during the entire experiment. The film was subjected to the following: annealing by two cycles of slow expansion and compression at $\pi < \pi_e$; incubation at 45 mN/m to confirm the absence of collapse at that π (green); rapid

Methods

Measurements of collapse

Our experiments measured rates of collapse by monomolecular films spread on the surface of captive bubbles. The bubbles floated in HSC against an agarose dome (38,39). The films formed by depositing solutions in chloroform at the air/water interface. Exhaustive exchange of the subphase removed the spreading solvent (39). Buffer pumped into or out of the subphase manipulated hydrostatic pressure, the size of the bubble, and its surface area. Analysis of the bubble's profile (40) provided π and the surface area. Temperature was the ambient value of 23°C.

Prior studies have shown that fluid monolayers collapse at rates that vary anomalously with π (39,41–43). The rates initially increase at π further above π_e but then reach a maximum at $\pi \approx 52$ mN/m and slow at higher π . To access higher π , at which the films become persistently metastable (42-44), rates of compression must exceed that fastest rate of collapse. The experiments here therefore measured isobaric collapse (45), with films held at $\pi = 52$ mN/m.

The structural integrity of the chamber containing the bubble limited the applied hydrostatic pressure to ≤3 atms. That restriction constrained compression of the films. To maximize the extent of isobaric measurements, the spread films had an initial π of 5–15 mN/m. After maximum expansion of the initial monolayer, two cycles of slow compression and expansion at $\pi < \pi_e$ annealed the films (Fig. 2 A). Incubation of the static bubble at approximately 45 mN/m confirmed the absence of collapse at that π (Fig. 2 A and B). A pulsed compression then increased π to 52 mN/m, after which measurements determined the change in surface area necessary to hold that π constant (Fig. 2 B and C).

Surface X-ray scattering

Our experiments measured GIXD at Sector 15-ID-C of the Advanced Photon Source at the Argonne National Laboratory (Argonne, IL, USA). Measurements recorded GIXD from monolayers formed at the air/water interface of a polytetrafluoroethylene Langmuir trough filled with HSC. The trough was mounted in a hermetically sealed, heliumfilled canister to minimize background scattering by oxygen, the level of which was monitored continuously, and maintained at <1%. Temperature was held at an ambient level of 23°C throughout the experiments. Aliquots of DPPC with variable amounts of cholesterol, dissolved in chloroform and deposited on the aqueous surface, increased π slightly above 0 mN/m. Compression then increased π to the values at which measurements were made.

GIXD provides information about the in-plane, lateral order of films. X-rays incident at a grazing angle penetrate only few nanometers below the surface (46). Scattering is therefore sensitive to the Langmuir monolayer rather than the bulk subphase. Measurements of GIXD used an X-ray beam with a wavelength (λ) of 1.24 Å. The incident angle corresponded to 0.85% of the critical value ($q_c = 0.0217 \text{ Å}^{-1}$). For an X-ray beam below the critical angle, the diffracted intensity is a function of the momentum transfer parallel to the interface, q_{xy} . At an angle of 2θ between the incident and scattered beams, q_{xy} is given by

$$q_{xy} = \frac{4\pi}{\lambda} \sin\left(\frac{2\theta}{2}\right).$$

compression to 52 mN/m (red); and then manipulation at that π (blue) to measure the rate of collapse. Area is expressed relative to the initial value (A_i) at which the film was spread. (B) π from the experiment in (A), expressed as a function of surface area. (C) Variation of area (left axis) and π (right axis) during the isobaric compression. Area and time are expressed relative to A_0 and t_0 when π first reached the isobaric value. To see this figure in color, go online.

The scattered intensity can be described in terms of diffraction from a large number of randomly oriented, two-dimensional crystalline domains. After subtracting background, the GIXD peaks were analyzed with the program OriginPro (Northampton, MA, USA) by fitting the data to one or two Lorentz-Gauss (1:1) crossed peaks. The q_{xy} of a fitted peak yielded the repeat distances between the diffracting hydrocarbon chains

$$d_{h,k} = \frac{2\pi}{q_{xy}}$$

for the Miller indices, h and k. The breadth of the peak provided the coherence length, L_{xy} , of the diffracting region according to the Sherrer formula (47)

$$L_{xy} = 0.9 \frac{2\pi}{\xi_{h,k}},$$

where $\xi = (\text{FWHM}^2 - \Delta^2)^{1/2}$ for a full width of the peak at the half-maximum (FWHM), and Δ is the resolution of the Soller slits. The acceptance of the Soller slits, fixed at 1.4 milliradians, determined errors in q_{xy} (9.56 \times 10⁻³ Å⁻¹).

For diffraction with two peaks, the following equation (48), using lattice spacings d_{11} and d_{02} corresponding to $\{(1,1),(1\overline{1})\}$ and $\{02\}$, determines the molecular tilt, τ , of chains toward their nearest neighbor:

$$d_{11} = \frac{d_{02}}{\left(\left(\frac{d_{02}^4}{A_0^2}\right)\cos^2\tau + \frac{1}{4}\right)^{\frac{1}{2}}},$$

where A_0 is the area of the unit cell.

RESULTS

Kinetics of collapse

Our experiments measured how different amounts of cholesterol affected the rates of collapse by spread monolayers of DPPC. To obtain quantitative data, we measured isobaric

collapse, with films held at constant π (Fig. 2). To the extent that any π corresponds to a unique interfacial concentration, the isobaric change in area is directly proportional to molecular adsorption or collapse (45). For a film that collapses completely with a fixed rate constant, the fractional rate at which area shrinks would be constant: (dA/A)/dt = -k. The semilogarithmic plot of area with time would be linear. Our results reasonably fit that behavior (Fig. 3 A). The slope of the linear fits provided the rate constant for collapse by films containing different amounts of cholesterol (Fig. 3 B). Rates of collapse for the films increased progressively with greater amounts of cholesterol (Fig. 3 B). The dose dependence was striking. The effect of cholesterol was limited below $X_{\text{chol}} = 0.20$. That result agreed with previous reports using different indications of collapse (49). Between $X_{\text{chol}} = 0.25$ and 0.30, the rate of collapse increased sevenfold.

GIXD

At $\pi=44$ mN/m, just below $\pi_{\rm e}$, GIXD from DPPC alone produced the expected two peaks at $q_{xy}\approx 1.42$ and $1.48~{\rm \AA}^{-1}$ (Fig. 4 A and B; Table 1), in agreement with previously published results at lower π (50). These peaks indexed as $\{0, 2\}$ and $\{(1,1), (1,\overline{1})\}$ of the centered rectangular unit cell. That structure had dimensions of $a=5.2~{\rm \AA}$ and $b=8.5~{\rm \AA}$ and an area of 44.5 or 22.2 ${\rm \AA}^2$ per alkyl chain. The scattered intensity from the $\{0,2\}$ peak was centered at $q_z\approx 0.55~{\rm \AA}^{-1}$ (Fig. 4 A and C), which indicated tilt of acyl chains toward nearest neighbors (35,46).

A similar pattern of GIXD persisted with $X_{\rm chol} = 0.05$ (Fig. 5 A; Table 1), indicating that the unit cell remained centered rectangular with acyl chains tilted toward nearest

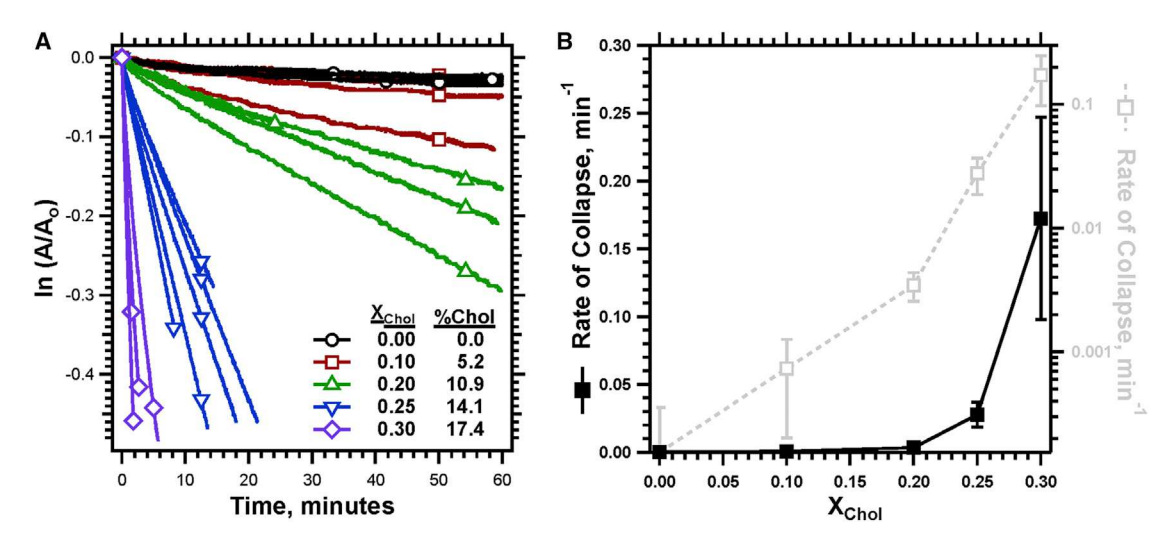


FIGURE 3 Dose-response of collapse for DPPC with different levels of cholesterol. (*A*) Semilogarithmic plots of area versus time during isobaric collapse at 23° C and $\pi = 52$ mN/m. The legend indicates the content of cholesterol both as mol fraction and as percentage of cholesterol (w:w). (*B*) Rate constants, obtained from the slopes of plots in (*A*), as a function of the content of cholesterol. Temperature = 23° C. Mean \pm SD. Some error-bars are smaller than the symbols. To see this figure in color, go online.

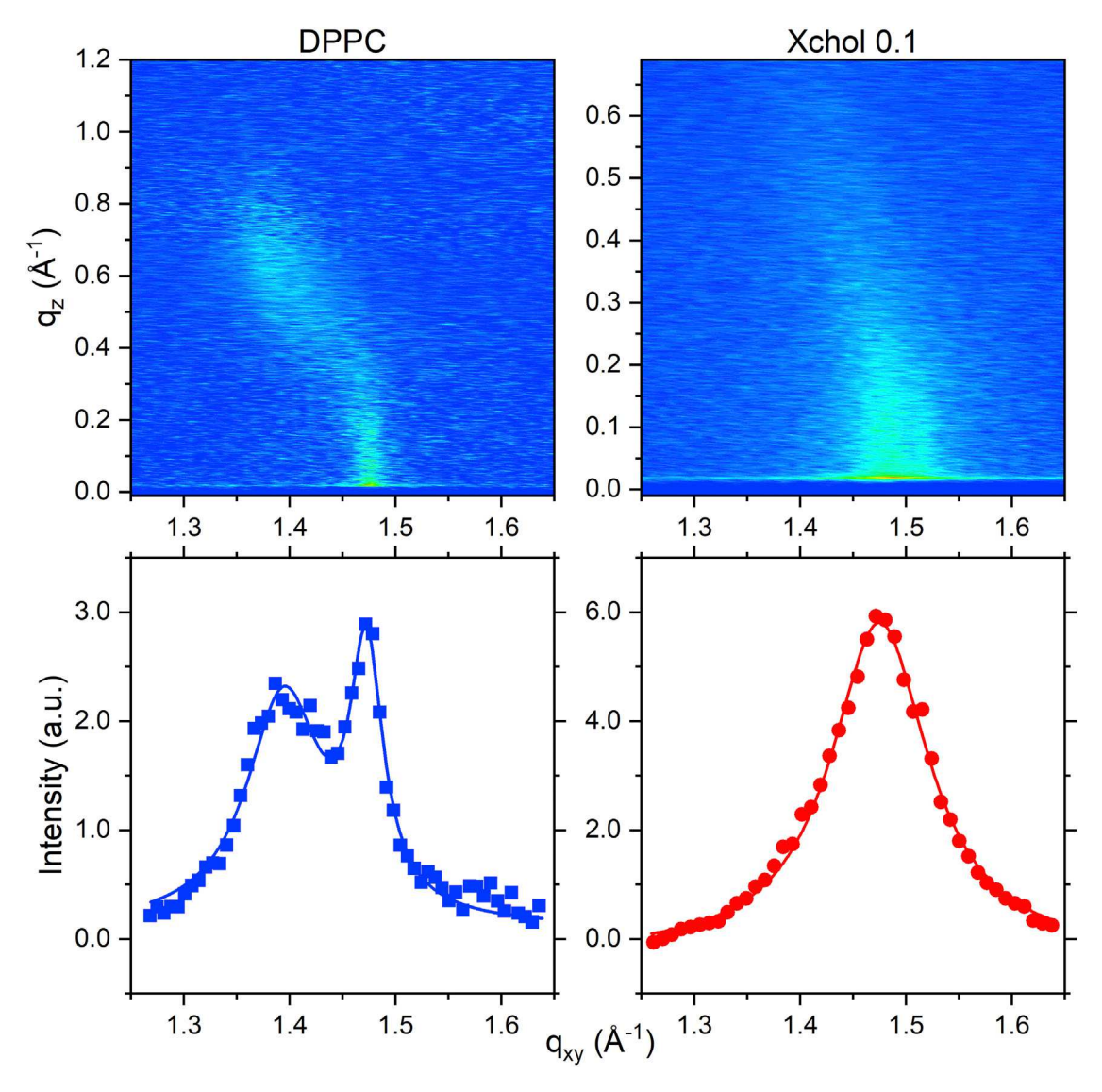


FIGURE 4 GIXD from monolayers of DPPC without and with ($X_{chol} = 0.10$) cholesterol. Measurements were made at $\pi \approx 44$ mN/m, just below $\pi_c \approx 40$ 46.5 mN/m, and an ambient temperature of 23°C. Top panels: imaged intensities. Bottom panels: intensities integrated over q_z at each q_{xy} . Symbols indicate measured values. Continuous curves give the best fit to one or two Gaussian distributions. To see this figure in color, go online.

neighbors. In contrast, at $X_{\text{chol}} = 0.10$, GIXD yielded a single, slightly asymmetric peak (Fig. 5 A) centered at $q_{\rm xy} \approx 1.48~{\rm \AA}^{-1}$ and $q_{\rm z} \approx 0~{\rm \AA}^{-1}$ (Table 1). The peak could be indexed as $\{(1,0), (0,1), (1,1)\}$ of the hexagonal lattice. Residual intensity from the {0,2} peak at $q_{xy} \approx 0.42 \text{ Å}^{-1}$ provided a reasonable explanation for the slight asymmetry. At $X_{\text{chol}} = 0.10$, conversion of the structure for DPPC alone—a centered rectangular structure with tilted chains—to a hexagonal unit cell without tilt was nearly complete.

Films with cholesterol above $X_{\text{chol}} = 0.10$ produced the same general pattern of diffraction (Fig 5 B). GIXD yielded a single peak. Over the range of $X_{\text{chol}} = 0.1-0.4$, the maximum intensity occurred at a value of $q_{xy} \approx 1.48 \text{ Å}^{-1}$ that was constant. The invariance of the peak position indicated that the spacing between the hydrocarbon chains remained fixed (Table 1). These results suggested that increased cholesterol had no effect on the stoichiometry of the ordered phase.

The increased cholesterol for $0.1 < X_{\text{chol}} < 0.4$ progressively broadened the GIXD peak (Fig. 5 B). Because larger crystalline regions produce sharper diffraction, this broadening showed that cholesterol produced smaller ordered regions. According to the Scherrer equation (methods), the greater FWHM indicated a decrease in the correlation length (L_{xy}) (Fig. 6; Table 1), defined as the distance over which a structure maintains positional order. These results showed that for the range of X_{chol} from 0.1 to 0.4, cholesterol caused a progressive decrease in the size of crystalline domains.

TABLE 1 Lateral organization of crystalline regions ($\pi=44$ mN/m)

$X_{ m chol}$	% Chol (w:w)	q_{xy} (Å ± 0.1)	a,b d-spacing (Å ± 0.01)	L_{xy} (A)	a, b (Å ± 0.1)	$A_{\rm UC} \ (\mathring{A}^2 \pm 0.1)$	τ (°)
0.00	0.0	1.39	$d_{(1,1), (1,\overline{1})} = 4.52$	65.6	a = 5.21	44.5	29.5
0.05	2.5	1.47	$d_{(0,2)} = 4.27$		b = 8.54	40.7	27.2
0.05	2.5	1.41 1.48	$d_{(1,1), (1,\overline{1})} = 4.46$ $d_{(0,2)} = 4.25$		a = 5.15 b = 8.49	43.7	27.3
0.10	5.2	1.47	4.27	48.2	a = 4.94	42.2	0
0.20	10.9	1.48	4.25	40.8	a = 4.90	41.6	0
0.30	17.4	1.47	4.27	33.6	a = 4.94	42.2	0
0.40	24.7	1.46	4.30	23.5	a = 4.97	42.8	0

Constituents were spread from solutions in chloroform and compressed. A_{UC} , area per unit cell; τ , angle of molecular tilt from the surface normal. ^aFor a centered rectangular unit cell, dimensions $a \neq b$.

Along with the decrease in the positional order of the condensed phase, the increased cholesterol also progressively reduced the maximum scattered intensity (Fig. 5 B). That change in part simply reflected the broadening of the GIXD peaks. The integrated intensities also decreased (Fig. 6). The progression with increasing cholesterol was less consistent than the decrease in the correlation length. The trend, however, was downward rather than upward, indicating that cholesterol reduced, rather than increased, the area occupied by the ordered phase.

DISCUSSION

Cholesterol produces an abrupt increase in rates of isobaric collapse by films of DPPC. At $X_{\rm chol} \leq 0.20$, collapse is detectable but not much greater than for DPPC alone. Between $X_{\rm chol} = 0.25$ –0.30, the rate increases by almost an order of magnitude. This behavior suggests that a small increase in cholesterol produces a major structural change, such as a phase transition.

The structural data indicate otherwise. At low $X_{\rm chol}$, our results show that cholesterol induces conversion of the centered rectangular phase of pure DPPC to a structure that has hexagonal symmetry. That transition, however, is virtually complete at $X_{\rm chol}=0.10$, well below the level that induces rapid collapse. The change in kinetics appears unrelated to that structural transition.

Our results suggest that over the range of $X_{\rm chol}$ in which collapse accelerates, the hexagonal ordered phase coexists with a disordered phase. Because GIXD detects only the ordered phase, the evidence is indirect. The invariance of the lattice parameter to the increased cholesterol is key. Prior studies show that at lower π , the ordered phase in films of DPPC/cholesterol can respond to changes in $X_{\rm chol}$ with an increase in chain-chain distances (50). The current studies, performed at significantly higher $\pi \approx \pi_{\rm e}$, show a different pattern. For $X_{\rm chol} = 0.1$ –0.4, the $q_{\rm xy}$ of the peak intensity remains constant. Despite the increased cholesterol in the film,

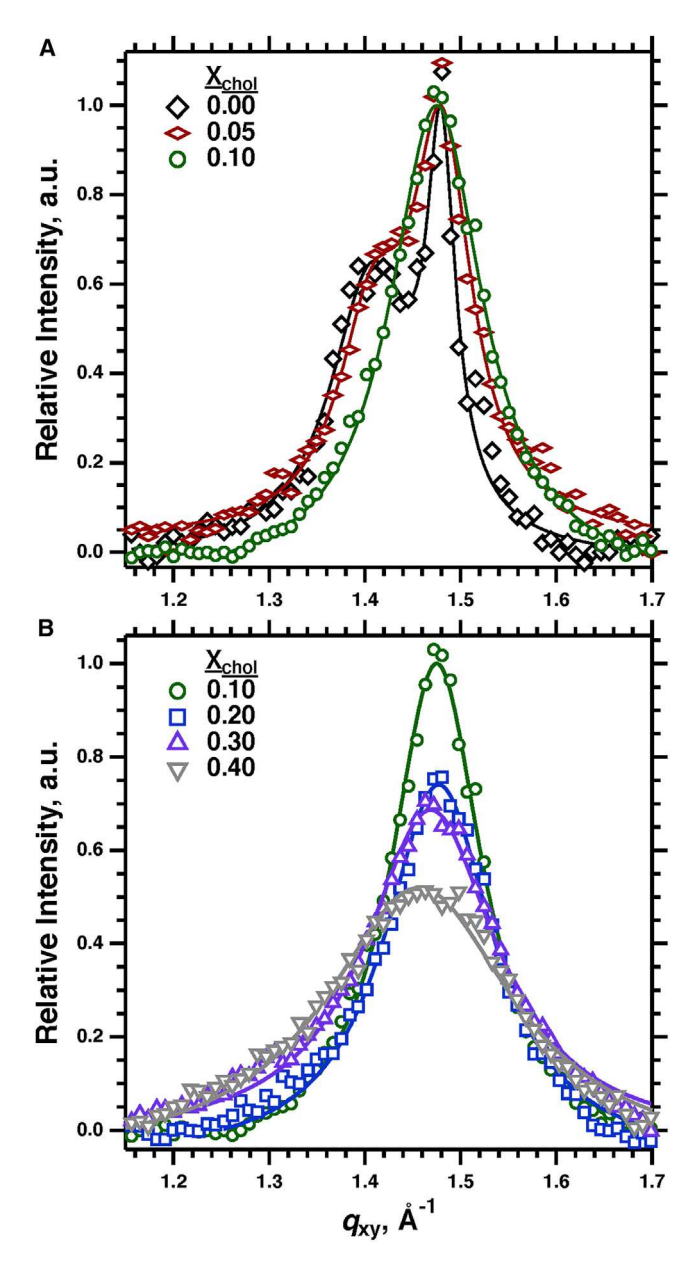


FIGURE 5 GIXD from films of DPPC with variable cholesterol. (A) $X_{\rm chol} = 0.00$ –0.10. Intensities are expressed relative to the maximum value of the fitted curve for each sample. (B) $X_{\rm chol} = 0.10$ –0.40. Intensities are normalized relative to the maximum value of the fitted curve for $X_{\rm chol} = 0.10$. For each panel, symbols give measured values. Continuous curves provide the best fit to one or two Gaussian distributions. Temperature = 23° C; $\pi = 45$ mN/m. To see this figure in color, go online.

the distances between chains in the ordered phase remain unchanged. For that range of $X_{\rm chol}$, the constant spacing strongly suggests that the stoichiometry in the ordered phase is also constant. Films with variable cholesterol cannot consist of a single phase with a fixed composition. The film must also contain a coexisting phase. A coexisting disordered structure would be undetected by GIXD.

The Gibbs phase rule provides a further restriction (51). At equilibrium, the chemical potential of each component

^bFor a hexagonal unit cell, a = b. A_{UC} contains two alkyl chains.

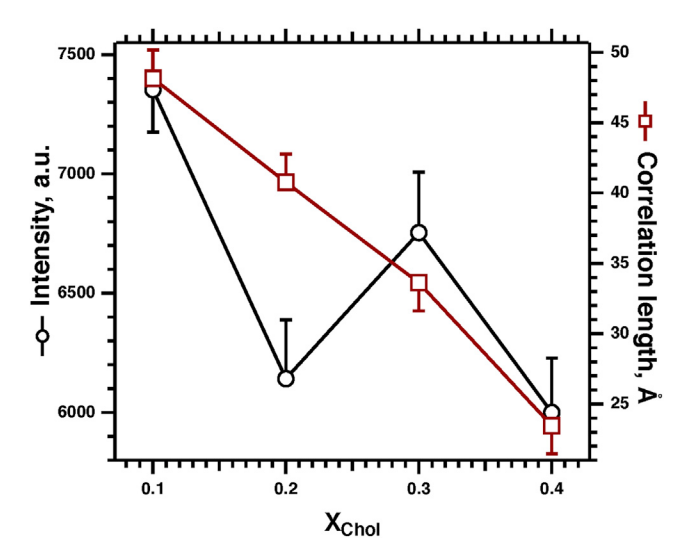


FIGURE 6 Dependence of the integrated, total scattered intensity (*left axis*) and correlation length (*right axis*) on content of cholesterol. Integration of the data in Fig. 5 B for $1.3 \le q_{\rm xy} \le 1.6$ yielded the intensities. Calculation of $L_{\rm xy}$ from the Scherrer equation used the full width of the peak at the half-maximum from those fits. To see this figure in color, go online.

must be equal in each phase. A two-component system with two phases and fixed intensive variables has no degrees of freedom. The areas of the two phases can vary, but not their compositions. The fixed stoichiometries require that added cholesterol must shift the relative areas of the two phases. The phase with a higher $X_{\rm chol}$ must expand. The regions with less cholesterol must shrink accordingly.

Our measured intensities suggest that cholesterol favors the disordered phase. For films exposed to a beam with the same flux and footprint, the relative area of the ordered phase determines the total scattered intensity. Our results suggest that more cholesterol produces less scattering. The dose response to cholesterol is imperfect, with an intensity at $X_{\rm chol}=0.3$ that is anomalously high. The variability may reflect the difficulty of integrating broad distributions. Although the intensity at any $q_{\rm xy}$ in the wings may be low, if they extend for a considerable range, small errors may have large effects. The trend and implications of our results, however, seem clear. Cholesterol generally produces less scattering, not more. The steroid partitions into the disordered phase and shrinks the area of the ordered regions.

The relationship between increased cholesterol and long-range positional order is simpler. Increasing $X_{\rm chol}$ progressively broadens the diffraction peaks (Fig 5 B), indicating a progressively lower correlation length (Fig. 6) and smaller crystalline domains. The abrupt increase in rates of collapse is unrelated to any change in the molecular structure of the ordered phase. The shift in kinetics results instead from smaller ordered crystallites that occupy a smaller fraction of the film.

The kinetics of collapse distinguish the different phases as solid and fluid. The ability of a two-dimensional film to

flow into the third dimension defines structures that collapse as fluid (52). Structures that resist collapse, and that are incapable of that flow, instead qualify as solids. That criterion, along with the structural results, determine that both the centered rectangular and hexagonal phases are solid ordered, although with different symmetries. The disordered phase that coexists with the hexagonal structure above $X_{\rm chol} = 0.25$ collapses readily and is therefore fluid. Analogy with the behavior of bilayers (53,54) raises the question of whether this coexisting phase is liquid-ordered, with extended acyl chains, or liquid-disordered. Our results show that the disordered phase is positionally disordered, but they provide no insight concerning the configuration of the chains.

The $X_{\rm chol}$ at which collapse increases corresponds roughly to the physiological value. The cholesterol-to-phospholipid ratio in calf surfactant is 83.6 nmol/µmol (1). DPPC represents ~33% of the phospholipids (36,37). Retaining the definition for the physiological mixture that $X_{\rm chol} = {\rm chol/(chol} + {\rm DPPC})$, $X_{\rm chol}$ for calf surfactant is 0.20. In the simplistic view that ignores all components in the physiological mixture other than cholesterol and DPPC, cholesterol in calf surfactant would fall just below the level at which the steroid becomes functionally detrimental. Any beneficial effect of cholesterol in a therapeutic surfactant could be achieved without increasing collapse as long as the level remained below the physiological content.

The localization of cholesterol to the disordered phase suggested by our results differs from findings in prior reports. Our own results with DPPC (50) and a study with extracted bovine surfactant (55) both found that in films with coexisting ordered and disordered phases, added cholesterol partitions at least partially into the ordered regions. The higher π of our current measurements provides an appealing explanation for the difference. Cholesterol, which prefers the ordered regions at lower π , is excluded from those structures in the more compressed films. This result emphasizes the importance for structural measurements of intensive variables, such as the π at which collapse begins. Structures at π well below π_e may have little significance in determining rates of collapse.

In summary, cholesterol has little effect on the kinetics of collapse by DPPC monolayers until $X_{\rm chol}$ reaches physiological levels. The striking acceleration of collapse at that level corresponds not to changes in the packing of the ordered phase but to a decrease in its long-range positional order and total area occupied by crystalline domains.

AUTHOR CONTRIBUTIONS

D.G., F.R.D., K.K., and M.J.F. participated in GIXD measurements. D.G., F.R.D., M.W.M., and W.B. analyzed the GIXD results. B.A.B. performed the measurements of collapse and analyzed the results and prepared the samples. S.B.H. planned the research, supervised the measurement and analysis of collapse, and wrote the manuscript. D.G. planned the research,

supervised the measurement and analysis of GIXD, and wrote the manuscript.

ACKNOWLEDGMENTS

Funds from the National Institutes of Health (HL130130 and 136734) supported this research. NSF's ChemMatCARS Sector 15 is supported by the Divisions of Chemistry (CHE) and Materials Research (DMR), National Science Foundation, under grant number NSF/CHE- 1834750. Use of the Advanced Photon Source, an Office of Science User Facility operated for the US Department of Energy (DOE) Office of Science by Argonne National Laboratory, was supported by the US DOE under contract no. DE-AC02-06CH11357.

DECLARATION OF INTERESTS

The authors declare no competing interests.

REFERENCES

- Hall, S. B., Z. Wang, and R. H. Notter. 1994. Separation of subfractions of the hydrophobic components of calf lung surfactant. *J. Lipid Res.* 35:1386–1394.
- Postle, A. D., E. L. Heeley, and D. C. Wilton. 2001. A comparison of the molecular species compositions of mammalian lung surfactant phospholipids. *Comp. Biochem. Physiol. A. Mol. Integr. Physiol.* 129:65–73.
- Bachofen, H., J. Hildebrandt, and M. Bachofen. 1970. Pressure-volume curves of air- and liquid-filled excised lungs-surface tension in situ. *J. Appl. Physiol.* 29:422–431.
- Horie, T., and J. Hildebrandt. 1971. Dynamic compliance, limit cycles, and static equilibria of excised cat lung. J. Appl. Physiol. 31:423–430.
- Valberg, P. A., and J. D. Brain. 1977. Lung surface tension and air space dimensions from multiple pressure-volume curves. *J. Appl. Physiol*. 43:730–738.
- Schürch, S., J. Goerke, and J. A. Clements. 1976. Direct determination of surface tension in the lung. *Proc. Natl. Acad. Sci. USA*. 73:4698– 4702.
- Wilson, T. A. 1981. Relations among recoil pressure, surface area, and surface tension in the lung. J. Appl. Physiol. 50:921–930.
- Schürch, S. 1982. Surface tension at low lung volumes: dependence on time and alveolar size. *Respir. Physiol.* 48:339–355.
- Smith, J. C., and D. Stamenovic. 1986. Surface forces in lungs. I. Alveolar surface tension-lung volume relationships. *J. Appl. Physiol*. 60:1341–1350.
- Gaines, G. L., Jr. 1966. Insoluble Monolayers at Liquid-Gas Interfaces. Interscience Publishers, p. 147.
- Schief, W. R., M. Antia, ..., V. Vogel. 2003. Liquid-crystalline collapse of pulmonary surfactant monolayers. *Biophys. J.* 84:3792–3806.
- Tierney, D. F., and R. P. Johnson. 1965. Altered surface tension of lung extracts and lung mechanics. J. Appl. Physiol. 20:1253–1260.
- Hildebran, J. N., J. Goerke, and J. A. Clements. 1979. Pulmonary surface film stability and composition. J. Appl. Physiol. 47:604–611.
- Notter, R. H., S. A. Tabak, and R. D. Mavis. 1980. Surface properties of binary mixtures of some pulmonary surfactant components. *J. Lipid Res.* 21:10–22.
- Enhorning, G., A. Shennan, ..., J. Milligan. 1985. Prevention of neonatal respiratory distress syndrome by tracheal instillation of surfactant: a randomized clinical trial. *Pediatrics*. 76:145–153.
- 16. Fujiwara, T., and B. Robertson. 1992. Pharmacology of exogenous surfactant. *In Pulmonary Surfactant: From Molecular Biology to Clinical Practice*. B. Robertson, E. M. G. V. Golde, and J. J. Batenburg, eds. Elsevier Science Publishers, pp. 561–592.

- Bernhard, W., J. Mottaghian, ..., C. F. Poets. 2000. Commercial versus native surfactants. Surface activity, molecular components, and the effect of calcium. Am. J. Respir. Crit. Care Med. 162:1524–1533.
- Bartmann, P., U. Bamberger, ..., L. Gortner. 1992. Immunogenicity and immunomodulatory activity of bovine surfactant (SF-RI 1). Acta Paediatr. 81:383–388.
- Gortner, L., U. Bernsau, ..., H. L. Reiter. 1990. A multicenter randomized controlled clinical trial of bovine surfactant for prevention of respiratory distress syndrome. *Lung.* 168:864–869.
- 20. Gortner, L., U. Bernsau, ..., H. L. Reiter. 1991. Does prophylactic use of bovine surfactant change drug utilization in very premature infants during neonatal period? *Dev. Pharmacol. Ther.* 16:1–6.
- Gortner, L., P. Bartmann, ..., F. Ball. 1992. Early treatment of respiratory distress syndrome with bovine surfactant in very preterm infants: a multicenter controlled clinical trial. *Pediatr. Pulmonol.* 14:4–9.
- 22. Woerndle, S., and P. Bartmann. 1994. The effect of three surfactant preparations on in vitro lymphocyte functions. *J. Perinat. Med.* 22:119–128.
- Andersson, J. M., C. Grey, ..., E. Sparr. 2017. Effect of cholesterol on the molecular structure and transitions in a clinical-grade lung surfactant extract. *Proc. Natl. Acad. Sci. USA*. 114:E3592–E3601.
- Bangham, A. D., N. G. A. Miller, ..., C. J. Morley. 1984. Introductory remarks about artificial lung expanding compounds (ALEC). *Colloids* Surf. 10:337–341.
- Durand, D. J., R. I. Clyman, ..., P. Ballard. 1985. Effects of a proteinfree, synthetic surfactant on survival and pulmonary function in preterm lambs. J. Pediatr. 107:775–780.
- 26. Häfner, D., P. G. Germann, and D. Hauschke. 1994. Effects of lung surfactant factor (LSF) treatment on gas exchange and histopathological changes in an animal model of adult respiratory distress syndrome (ARDS): comparison of recombinant LSF with bovine LSF. *Pulm. Pharmacol.* 7:319–332.
- Cochrane, C. G., and S. D. Revak. 1994. Protein-phospholipid interactions in pulmonary surfactant. The Parker B. Francis lectureship. *Chest*. 105:57S–62S.
- 28. Robertson, B. 1984. Pathology and pathophysiology of neonatal surfactant deficiency ("respiratory distress syndrome," "hyaline membrane disease"). *In Pulmonary Surfactant*. B. Robertson, L. M. G. Van Golde, and J. J. Batenburg, eds. Elsevier Science Publishers, pp. 383–418.
- Gross, N. J. 1995. Pulmonary surfactant: unanswered questions. *Tho-rax*. 50:325–327.
- Kribs, A. 2016. Minimally invasive surfactant therapy and noninvasive respiratory support. Clin. Perinatol. 43:755–771.
- Cummings, J. J., E. Gerday, ..., I. Aero-02 Study. 2020. Aerosolized calfactant for newborns with respiratory distress: a randomized trial. *Pediatrics*. 146:e20193967.
- Gunasekara, L., S. Schürch, ..., M. Amrein. 2005. Pulmonary surfactant function is abolished by an elevated proportion of cholesterol. *Biochim. Biophys. Acta.* 1737:27–35.
- Clements, J. A. 1977. Functions of the alveolar lining. *Am. Rev. Respir. Dis.* 115 (6 Part II):67–71.
- 34. Bangham, A. D., C. J. Morley, and M. C. Phillips. 1979. The physical properties of an effective lung surfactant. *Biochim. Biophys. Acta.* 573:552–556.
- 35. Kaganer, V. M., H. Möhwald, and P. Dutta. 1999. Structure and phase transitions in Langmuir monolayers. *Rev. Mod. Phys.* 71:779–819.
- Kahn, M. C., G. J. Anderson, ..., S. B. Hall. 1995. Phosphatidylcholine molecular species of calf lung surfactant. Am. J. Physiol. 269:L567– L573.
- 37. Markin, C. J., and S. B. Hall. 2021. The anionic phospholipids of bovine pulmonary surfactant. *Lipids*. 56:49–57.
- Putz, G., J. Goerke, ..., J. A. Clements. 1994. Evaluation of pressuredriven captive bubble surfactometer. J. Appl. Physiol. 76:1417–1424.

- 39. Crane, J. M., G. Putz, and S. B. Hall. 1999. Persistence of phase coexistence in disaturated phosphatidylcholine monolayers at high surface pressures. Biophys. J. 77:3134-3143.
- 40. Khoojinian, H., J. P. Goodarzi, and S. B. Hall. 2012. Optical factors in the rapid analysis of captive bubbles. *Langmuir.* 28:14081–14089.
- 41. Rugonyi, S., E. C. Smith, and S. B. Hall. 2004. Transformation diagrams for the collapse of a phospholipid monolayer. Langmuir. 20:10100-10106.
- 42. Smith, E. C., J. M. Crane, ..., S. B. Hall. 2003. Metastability of a supercompressed fluid monolayer. Biophys. J. 85:3048-3057.
- 43. Smith, E. C., T. G. Laderas, ..., S. B. Hall. 2004. Persistence of metastability after expansion of a supercompressed fluid monolayer. Langmuir. 20:4945-4953.
- 44. Crane, J. M., and S. B. Hall. 2001. Rapid compression transforms interfacial monolayers of pulmonary surfactant. Biophys. J. 80:1863–1872.
- 45. Smith, R. D., and J. C. Berg. 1980. The collapse of surfactant monolayers at the air-water interface. J. Colloid Interface Sci. 74:273–286.
- 46. Als-Nielsen, J., D. Jacquemain, ..., L. Leiserowitz. 1994. Principles and applications of grazing incidence X-ray and neutron scattering from ordered molecular monolayers at the air-water interface. Phys. Rep. 246:251-313.
- 47. Borie, B. 1965. X-ray diffraction in crystals, imperfect crystals, and amorphous bodies. J. Am. Chem. Soc. 87:140–141.

- 48. Tippmann-Krayer, P., and H. Moehwald. 1991. Precise determination of tilt angles by X-ray diffraction and reflection with arachidic acid monolayers. Langmuir. 7:2303-2306.
- 49. Colacicco, G., and M. K. Basu. 1977. Effects of cholesterol and cholesteryl ester on dynamic surface tension of dipalmitoyl lecithin. J. Colloid Interface Sci. 61:516–518.
- 50. Ivankin, A., I. Kuzmenko, and D. Gidalevitz. 2010. Cholesterol-phospholipid interactions: new insights from surface x-ray scattering data. Phys. Rev. Lett. 104:108101.
- 51. Callen, H. B. 1960. Thermodynamics; an Introduction to the Physical Theories of Equilibrium Thermostatics and Irreversible Thermodynamics. Wiley, pp. 163-167.
- 52. Rapp, B., and H. Gruler. 1990. Phase-transitions in thin smectic films at the air-water interface. Phys. Rev. A. 42:2215-2218.
- 53. Ipsen, J. H., G. Karlström, ..., M. J. Zuckermann. 1987. Phase equilibria in the phosphatidylcholine-cholesterol system. Biochim. Biophys. Acta. 905:162-172.
- 54. McConnell, H. M., and M. Vrljic. 2003. Liquid-liquid immiscibility in membranes. Annu. Rev. Biophys. Biomol. Struct. 32:469-492.
- 55. Keating, E., L. Rahman, ..., N. O. Petersen. 2007. Effect of cholesterol on the biophysical and physiological properties of a clinical pulmonary surfactant. Biophys. J. 93:1391-1401.